Chapter 4
Non-radiative Processes in Nanocrystals

J. M. Collins

Abstract This paper discusses non-radiative processes relevant to the luminescence characteristics of optically active ions doped into insulators or large-gap semiconductors, with particular attention to how these processes are affected as the particle size is reduced from bulk single crystals to as small as a few nanometers. The non-radiative processes discussed in this article are thermal line broadening and thermal line shifting, relaxation via phonons between excited electronic states, and vibronic emission and absorption. One prominent effect of confinement in the systems of interest is a reduction in the phonon density of states. Thus, we focus on how these non-radiative processes are altered due to the change in the phonon density of states as particle size decreases.

4.1 Introduction

Inorganic insulators doped with rare-earth ions and transition metal ions represent an important class of luminescent materials for many applications, including phosphors for lighting, scintillators, solid-state laser materials, bio-markers for imaging, and nanothermometry. Following excitation by radiation, the optical ions usually undergo some degree of non-radiative relaxation, releasing part or all of its energy to the lattice. During the non-radiative relaxation, all or part of the electronic energy initially stored in the optically active ion is converted into phonons.

The specific non-radiative processes addressed in this work are thermal line broadening, thermal line shifting, decay via a phonon from one electronic level to another, vibronic transitions, and phonon-assisted energy transfer. Generally speaking, the two main effects of going from the bulk to the nano are: (1) an increase in the surface to volume ratio, and (2) a reduction in the phonon density of states. In this paper we focus on the second point. Most non-radiative processes that play a significant role in the luminescent properties of these systems involve phonons, and most of those are determined in part by the phonon density of states of the

J.M. Collins (✉)

Department of Physics and Astronomy, Wheaton College, Norton, MA 02766, USA
e-mail: jcollins@wheatonma.edu

lattice. One goal of this paper is to present results that demonstrate how the reduced density of states in nanoparticles affect the aforementioned processes, and under what conditions will such affects be noticeable.

Before doing so, however, we present some detailed theory of the non-radiative processes in solids, including various forms of the adiabatic approximation, the non-adiabatic operators that drive the transitions, and prediction about the rates of non-radiative transitions. The electron-phonon coupling is a central idea to the theory. We consider primarily systems where this coupling is weak, such as f-f transitions of rare earth ions.

To set up the problem, we first address the following question: How is the energy stored in the electronic system of the optically active ion converted into phonons? To answer this question, it is useful to first review the notion of an adiabatic process.

4.2 Adiabatic Processes

In this section, we introduce the *Adiabatic Approximation*, which allows separation of the motion of the nuclei from that of the electrons. The idea of an *adiabatic* process is fundamental to Quantum Mechanics and Thermodynamics, and so a brief review of an adiabatic process, is useful. For interested readers, the original proof of the adiabatic theorem by Max Born is given in Ref. [1].

Suppose we have a system with a Hamiltonian having the time dependence shown in Fig. 4.1. At $t < t_i$, the Hamiltonian is constant at H_i, and at $t > t_f$, the Hamiltonian is constant at H_f, and during a time $\Delta t = t_f - t_i$ the Hamiltonian is time-dependent. Suppose also that the system has a characteristic time T. (For example, if the system were a harmonic oscillator, T would represent the period of the oscillator.) In an adiabatic process, we demand that the following three conditions hold.

1. Suppose there exists another state $|m\rangle$ nearby to $|n\rangle$ with an energy ε_m. The variation in the Hamiltonian during the time Δt must be less than or on the order of $\varepsilon_n - \varepsilon_m$: $\langle H_f - H_i \rangle <\sim |\varepsilon_n - \varepsilon_m|$.
2. The time over which the Hamiltonian varies must be much greater than the characteristic time of the system: $\Delta t \gg T$

Fig. 4.1 Generic diagram of a time-dependent Hamiltonian between $t_{initial}$ and t_{final}. In this diagram, the Hamiltonian varies linearly with time, but a linear dependence is not required for the system to vary adiabatically
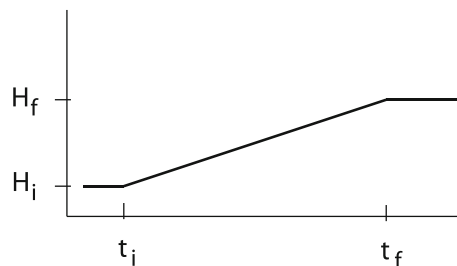
3. The initial state $\left|n\right\rangle$ of the system is nondegenerate.

Consider s system for which the above conditions hold, and that at $t < t_i$ such a system is in the stationary state $\left|n\right\rangle$ with an energy ε_n, i.e., $H_i\left|n\right\rangle = \varepsilon_n\left|n\right\rangle$. The Adiabatic Approximation states that, although the time dependence of the Hamiltonian causes the system to evolve during the time Δt, the system will remain in the state $\left|n\right\rangle$ throughout. At $t = t_f$ the energy of the system will be ε'_n, (i.e., $H_f\left|n\right\rangle = \varepsilon'_n\left|n\right\rangle$), where in general $\varepsilon'_n \neq \varepsilon_n$. The wavefunction represented by the state $\left|n\right\rangle$ will also have changed during the time Δt. That is, if we define $\langle x \mid n \rangle = \psi_n$, then in general $\psi_n^i \neq \psi_n^f$.

As an elementary example, consider the case of an electron trapped in an infinite, one-dimensional well. For a particle of mass m and a box with potential energy is zero region between $x = 0$ and $x = L$, the energies and wavefunctions of the system are given by

$$\varepsilon_n = \frac{h^2\pi^2}{8 \text{ mL}^2} n^2 \text{ and } \psi(x) = \sqrt{\frac{2}{L}} \sin\left(\frac{n\pi x}{L}\right), \qquad (4.1)$$

where $n = 1, 2, 3, \ldots$ is the quantum number of the state of the system. The characteristic time of the particle in the nth state is associated with the round trip time, T_n, between $x = 0$ and $x = L$, and is given by $T_n \approx h/\varepsilon_n$.

Suppose now that the wall of the box at $x = L$ is moved slowly (adiabatically) in a time $\Delta t \gg T_n$ to a final position $x = 2 L$. During that time, the size of the box can be described by the function $l(t)$ such that $l(t_i) = L$ and $l(t_i + \Delta t) = 2 L$. Figure 4.2a shows the particle's wavefunction (in the $n = 1$ state) at t_i and at t_f. Note that as the wall is moved, the particle remains in the $n = 1$ state, as long as the wall is moved slowly.

In this scenario, the system consists of a slow subsystem (the expanding box) and a fast subsystem (the particle). As the wall moves, the particle responds nearly instantaneously to the new position of the wall, and always remains in the nth energy state; a transition from the nth to the state $(n + 1)th$ state (or any other state) will not occur. During the time Δt, the instantaneous energy and wavefunction of the system are given by:

$$\varepsilon_n(l) = \frac{h^2\pi^2}{8m(l(t))^2} n^2 \text{ and } \psi(x, l) = \sqrt{\frac{2}{l(t)}} \sin\left(\frac{n\pi x}{l(t)}\right) \qquad (4.2)$$

As the wall moves, the wavefunctions and energies have a dependence on l, the width of the box, and hence on time. Because the form of the energies and wavefunctions are unaltered, this dependence on the length of the box is a *parametric* one.

a

b
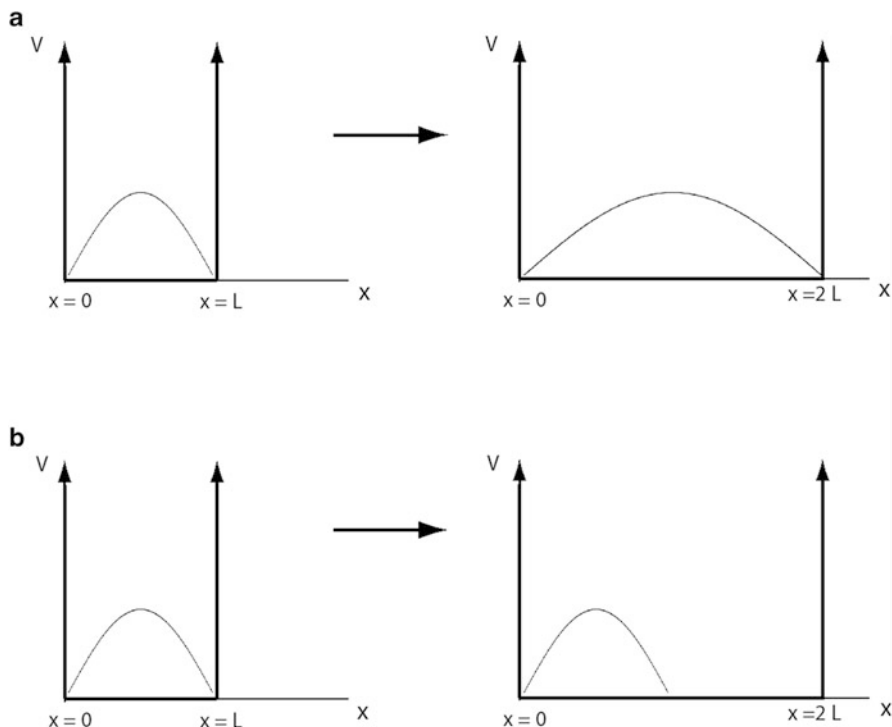
Fig. 4.2 (**a**) In an adiabatic process the wall moves from x = L to x = 2L, the particle remains in the same state, and the wavefunction adapts adiabatically. (**b**) If the wall is moved suddenly, the initial wavefunction is unchanged immediately after the wall is moved. In each case above the n = 1 wavefunction is shown

For the sake of comparison, it is useful to consider briefly the case where the wall moves suddenly (i.e. non-adiabatically) from $x = L$ to $x = 2L$ in a time $\Delta t \ll T_n$. This case is shown in Fig. 4.2b. In this case, the particle does not have time to react to the movement of the wall. Immediately after the wall is moved, the wavefunction of the particle is unaltered, and the particle is now in a superposition state consisting of many stationary states of the box of length 2L. The motion of the wall in this case is decidedly non-adiabatic.

4.3   Ion in a Solid: The Adiabatic Approximation

An optically active of ion embedded in a solid consists of two subsystems: the electrons and the nuclei. Because the ratio of the nuclear mass to the electronic mass is on the order of 10^5, the nuclei move more slowly than the electrons by a factor

of 10^{-2}–10^{-3}. Thus, the electrons and the nuclei constitute a fast subsystem and a slow subsystem, respectively, and an adiabatic approximation is indeed justified.

Treatments in the literature on the adiabatic approximation as applied to molecules or to ions in a solid are plentiful, [e.g. 2–9]. Though different authors each present valid treatments of the adiabatic approximation, there are inconsistencies among them, particularly in the nomenclature. For an excellent overview of the distinctions between some of the treatments, see the article by Azumi and Matsuzaki [6].

4.3.1   The Full Hamiltonian

The Hamiltonian of a molecular system can be expressed as

$$H_{total} = T_e(r) + T_N(R) + U(r,R) + V(R),\tag{4.3}$$

where

$$T_e(r) = \sum_i \frac{p_i^2}{2m} = -\frac{\hbar^2}{2m}\sum_i \vec{\nabla}_i^2\tag{4.4}$$

$$T_N(R) = \sum_i \frac{P_\alpha^2}{2M_\alpha} = -\frac{\hbar^2}{2}\sum_\alpha \frac{\vec{\nabla}_\alpha^2}{M_\alpha}\tag{4.5}$$

$$U(r,R) = \sum_i\sum_{j>i} \frac{e^2}{\left|\vec{r}_i - \vec{r}_j\right|} + \sum_i\sum_\alpha \frac{Z_\alpha e^2}{\left|\vec{r}_i - \vec{R}_\alpha\right|}\tag{4.6}$$

$$V(R) = \sum_\alpha\sum_{\beta>\alpha} \frac{Z_\alpha Z_\beta e^2}{\left|\vec{R}_\alpha - \vec{R}_\beta\right|}\tag{4.7}$$

In the equations above, $\vec{r}_i$ and $\vec{r}_j$ are the positions of the electrons, and $\vec{R}_\alpha$ and $\vec{R}_\beta$ are the positions of the nuclei. $T_e(r)$ and $T_N(R)$ are the kinetic energy operators for the electrons and nuclei, respectively. $U(r,R)$ contains the electron-electron and electron-nuclear interactions, and $V(R)$ is represents the repulsive interaction between the nuclei. Z_α and M_α are the atomic number and mass of the αth nucleus, respectively, and m is the mass of the electron. To simplify the notation, for the remainder of the article we will use the symbols r and R instead of $\vec{r}$ and $\vec{R}$.

The eigenstates and eigenvalues of the system are given by the solutions to the time-independent Schrodinger equation:

$$(H_{total} - E_{total})\,\Psi(r,R) = 0\tag{4.8}$$

Because of the electron-nuclear interaction term, the Hamiltonian H_{total} does not allow for separation of variables, i.e., $\Psi(r, R)$ cannot be separated into the product of electronic and nuclear wavefunctions.

4.3.2 The Born-Oppenheimer Adiabatic Approximation

Let us define an electronic Hamiltonian consisting all the terms containing the electronic coordinates,

$$H_{elec} = T_e(r) + U(r, R) \ . \tag{4.9}$$

As constructed, the potential energy term in H_{elec} contains both electronic and nuclear positions, so the eigenfunctions of H_{elec} will be functions of both r and R.

Let us assume that at any moment the nuclear positions can be considered fixed, that is, the electrons are "unaware" of the nuclear motion. This assumption is justified by the fact that the nuclei move much more slowly than the electrons, so that the electrons can react instantaneously to any change in position of the nuclei. (Note that the nuclear motion in this system is the analog to the moving wall in the previous section.) In such an assumption, R is treated as a parameter and r as the variable. The Schrodinger equation for H_{elec} becomes

$$(T_e(r) + U(r, R) - \epsilon_k(R)) \phi_k(r, R) = 0. \tag{4.10}$$

The wavefunctions $\phi_k(r, R)$ and the eigenvalues $\epsilon_k(R)$ correspond to the *kth* electronic state at a particular set of nuclear coordinates. As the nuclear coordinates change, the system remains in the *kth* electronic state as the wavefunction and energy eigenvalues adjust adiabatically. The set of wavefunctions $\phi_k(r, R)$ may be chosen to form a complete, orthonormal set, i.e., they obey the following relationship:

$$\langle \phi_i(r, R) \phi_j | (r, R) \rangle = \delta_{ij}. \tag{4.11}$$

Combining Eqs. (4.3), (4.8), and (4.9), we may write:

$$(T_N(R) + V(R) + H_{elec} - E_{total}) \Psi(r, R) = 0 \tag{4.12}$$

We see that the Hamiltonian is a sum of terms that depend on the nuclear and electronic coordinates separately. Since the $\phi_k(r, R)$ form a complete set, $\Psi(r, R)$ may be expanded as follows:

$$\Psi(r, R) = \sum_k \phi_k(r, R) \chi_k(R), \tag{4.13}$$

where the $\chi_k(R)$ are expansion coefficients that are functions of the nuclear positions.

Inserting (4.13) into (4.12), and writing the electronic state in Dirac notation, we obtain:

$$(T_N(R) + V(R) + H_{elec} - E_{total}) \sum_k \chi_k(R) \, |\phi_k(r, R)\rangle = 0 \qquad (4.14)$$

Operating on Eq. (4.14) on the left with $\langle \phi_i(r, R) \, |$, and using (4.5), (4.9), (4.10) and (4.11), we get:

$$[T_N(R) + V(R) + \epsilon_i(R) - E_{total}] \, \chi_i(R)$$

$$- \sum_k \sum_\alpha \frac{\hbar^2}{2M_\alpha} \chi_k(R) \, \langle \phi_i(r, R) | \, \overrightarrow{\nabla}_\alpha^2 \, |\phi_k(r, R)\rangle$$

$$- \sum_k \sum_\alpha \frac{\hbar^2}{M_\alpha} \langle \phi_i(r, R) | \, \overrightarrow{\nabla}_\alpha \, |\phi_k(r, R)\rangle \, \overrightarrow{\nabla}_\alpha \chi_k(R) = 0 \qquad (4.15)$$

In arriving at (4.15) we integrated over all electronic coordinates, i.e. we imposed the orthonormality condition defined by Eq. (4.11), so $\epsilon_i(R)$ does not depend on the electronic coordinates. We also used the following:

$$\overrightarrow{\nabla}_\alpha^2 \phi(r, R) \, \chi(R) = \overrightarrow{\nabla}_\alpha \cdot \left[\overrightarrow{\nabla}_\alpha (\phi \chi) \right]$$

$$= \overrightarrow{\nabla}_\alpha \cdot \left(\phi \overrightarrow{\nabla}_\alpha \chi + \chi \overrightarrow{\nabla}_\alpha \phi \right)$$

$$= \phi \overrightarrow{\nabla}_\alpha^2 \chi + \chi \overrightarrow{\nabla}_\alpha^2 \phi + 2 \left(\overrightarrow{\nabla}_\alpha \phi \right) \cdot \left(\overrightarrow{\nabla}_\alpha \chi \right)$$

The term in brackets [] on the left side of Eq. (4.15) depends only on the nuclear positions. The last two terms in Eq. (4.15) contain derivatives of the electronic wavefunctions with respect to the nuclear positions, and are responsible for coupling the nuclear and electronic subsystems.

We now make the assumption that the last two terms on the right side of Eq. (4.15) are negligible, simplifying Eq. (4.15) to

$$[T_N(R) + V(R) + \epsilon_i(R) - E_{total}] \, \chi_i(R) = 0 \qquad (4.16)$$

Equation (4.16) is essentially the Schrodinger equation for the nuclear wavefunctions, $\chi_i(R)$. Note that $\epsilon_i(R)$ comes from the solution to the electronic Schrodinger Eq. (4.10) and plays the role of a potential energy in (4.16).

Neglecting the last two terms in (4.15) has allowed for the separation of the electronic and nuclear wavefunctions whose solutions are found by first solving

Eq. (4.10) and then (4.16). Consequently, the wavefunction of the system can be written as the product of an electronic wavefunction and a nuclear wavefunction:

$$\Psi_k(r, R) = \phi_k(r, R) \chi_k(R) \tag{4.17}$$

Equations (4.10), (4.13) and (4.17) comprise the *Born-Oppenheimer Adiabatic Approximation*. In this approximation, $\epsilon_i(R)$ corresponds to an average electronic potential in which the nuclei move, and includes, as seen from Eq. (4.10), the kinetic energy of the electrons, the electron-electron interaction, and the electron-nuclear interaction. If the nuclear positions change, the electrons, with their much smaller masses, react immediately to the new position of the nuclei, producing a new $\epsilon_i(R)$, that is, the system behaves adiabatically in response to the motion of the nuclei.

The validity of the Born-Oppenheimer Adiabatic Approximation rests on the last two terms in (4.15) to be considered negligible, that is, on terms of the form $\overrightarrow{\nabla}_\alpha \phi_k(r, R)$ and $\overrightarrow{\nabla}_\alpha^2 \phi_k(r, R)$, and on the nuclear mass, M_α. Neglecting the terms containing $\overrightarrow{\nabla}_\alpha \phi_k(r, R)$ and $\overrightarrow{\nabla}_\alpha^2 \phi_k(r, R)$ assumes a weak dependence of the electronic wavefunction, $\phi_k(r, R)$, on the nuclear coordinates. Specifically, it assumes that the slope and the curvature of $\phi_k(r, R)$ in R-space are small. This is reasonable for many systems, especially if the amplitudes of the vibrations of the nuclei are small. Also, the large nuclear mass M_α in the denominator contributes to making the last two terms in (4.15) small perturbations to the Hamiltonian in (4.16).

4.3.3 The Born-Huang Adiabatic Approximation

In this section we relax slightly the constraints of the Born-Oppenheimer approximation. Recall that in adiabatic process the motion of the slow subsystem will not induce a change in the state of the fast subsystem. Thus, if the fast system is perturbed by an interaction with slow system, only matrix elements that connect two different electronic states can induce the system to transition to a different electronic state. In examining Eq. (4.15), one notices that only the off diagonal components of matrix elements in the last two terms of Eq. (4.15) connect different electronic states. The diagonal components, on the other hand, connect each electronic state to itself, and so can be incorporated into the Hamiltonian in (4.16).

Following this thought, we first consider the diagonal component of the last term in Eq. (4.15):

$$-\frac{\hbar^2}{M_\alpha} \left\langle \phi_k(r, R) \left| \overrightarrow{\nabla}_\alpha \right| \phi_k(r, R) \right\rangle \overrightarrow{\nabla}_\alpha \chi_k(R) \tag{4.18}$$

where $\left\langle \phi_i(r, R) \left| \overrightarrow{\nabla}_\alpha \right| \phi_k(r, R) \right\rangle$ represents an integral over electronic coordinates, r, and can be rewritten as

$$-\frac{\hbar^2}{M_\alpha}\left[\int \phi_k\,(r,R)\,\vec{\nabla}_\alpha\phi_k\,(r,R)\,d\vec{r}\right]\vec{\nabla}_\alpha\chi_k(R) \tag{4.19}$$

Inside the brackets [] in the above expression, we may rearrange the integration over $\vec{r}$ with the derivative with respect to the nuclear coordinates to obtain

$$-\frac{\hbar^2}{M_\alpha}\vec{\nabla}_\alpha\left[\int \phi_k\,(r,R)\,\phi_k\,(r,R)\,d\vec{r}\right]\vec{\nabla}_\alpha\chi_k(R) \tag{4.20}$$

Imposing orthonormality of the electronic states (at all R), (4.20) is equal to zero, since $\vec{\nabla}_\alpha(1) = 0$. Thus, the diagonal matrix elements of the last term in (4.15) are identically zero.

We now consider the diagonal elements of the second term in Eq. (4.15), namely

$$-\frac{\hbar^2}{2M_\alpha}\chi_k(R)\langle\phi_k\,(r,R)\,\left|\vec{\nabla}^2_\alpha\right|\phi_k\,(r,R)\rangle. \tag{4.21}$$

We may choose $\phi_k(r,R)$ to the real, in which case the integral form of (4.21) appears as

$$-\frac{\hbar^2}{2M_\alpha}\chi_k(R)\int \phi_k\,(r,R)\,\vec{\nabla}^2_\alpha\phi_k\,(r,R)\,d\vec{r}. \tag{4.22}$$

To evaluate (4.22), consider the identity

$$0 = \nabla^2_\alpha\left[\int \phi_k\,(r,R)\,\phi_k\,(r,R)\,d\vec{r}\right]$$

$$= \int \nabla^2_\alpha\,[\phi_k\,(r,R)\,\phi_k\,(r,R)]\,d\vec{r}$$

$$= 2\int \left(\vec{\nabla}_\alpha\phi_k\,(r,R)\right)^2 d\vec{r} + 2\int \phi_k\,(r,R)\,\nabla^2_\alpha\phi_k\,(r,R)\,d\vec{r} \tag{4.23}$$

where in the first line above we have use the orthonormality condition (4.11). Using (4.23), (4.22) can be written as

$$\frac{\hbar^2}{2M_\alpha}\chi_k(R)\int \left(\vec{\nabla}_\alpha\phi_k\,(r,R)\right)^2 d\vec{r}. \tag{4.24}$$

Thus, the diagonal elements of the last two terms in (4.15) are reduced to (4.24). In carrying out the integration over $\vec{r}$ in (4.24) results in a term that is a function of R only, and so may be incorporated into the left side of Eq. (4.16), which becomes

$$\left[T_N(R) + V'(R) + \epsilon_k(R) - E'_{total}\right]\chi_k(R) = 0, \tag{4.25}$$

where

$$V'(R) = V(R) + \frac{\hbar^2}{2M_\alpha} \int \left(\overrightarrow{\nabla}_\alpha \phi_k(r, R) \right)^2 d\overrightarrow{r}. \tag{4.26}$$

Equation (4.25) can be solved to obtain the nuclear wavefunctions, $\chi_k(R)$. As previously done, the separation of the electronic and nuclear equations allows us to write the states of the system as

$$\Psi_k(r, R) = \phi_k(r, R) \chi_k(R). \tag{4.27}$$

where the $\chi_k(R)$ in (4.27) are different than those in (4.17). Equations (4.10), (4.25), and (4.27) define the *Adiabatic Approximation*, sometimes referred to as the *Born-Huang Adiabatic Approximation*. Equation (4.25) represents a slight improvement over (4.16).

4.3.4   The Crude Adiabatic Approximation

It will prove useful to consider one additional form of the adiabatic approximation. We begin by rewriting (4.9) as follows:

$$H_{elec} = T_e(r) + U(r, R_0) + \Delta U(r, R)$$
$$= H^0_{elec}(r, R_0) + \Delta U(r, R) \tag{4.28}$$

where R_0 indicates the nuclei are at fixed positions, and $\Delta U(r, R)$ is the interaction due to the displacements of the nuclei from those positions. Neglecting $\Delta U(r, R)$, and using the same arguments as in Sect. 4.3.2, the electronic wavefunctions can be found by solving the Schrodinger equation

$$\left(T_e(r) + U(r, R_0) - \epsilon_i^0(R_0) \right) \phi_k^0(r, R_0) = 0, \tag{4.29}$$

which is analogous to Eq. (4.10). In (4.29), the $\phi_k^0(r, R_0)$ are electronic wavefunctions with the nuclei at fixed positions, and are not identical to the analogous terms in (4.10). These $\phi_k^0(r, R_0)$ also form a complete set of orthonormal wavefunctions, so

$$\Psi_k(r, R) = \sum_k \phi_k^0(r, R_0) \chi_k(R), \tag{4.30}$$

with the understanding that the $\chi_k(R)$ in (4.26) are not the same as those in (4.13). The states defined in (4.26) are called the *crude* Born-Oppenheimer states.

Following arguments similar to those in Sect. 4.2.2, the Schrodinger equation analogous to (4.16), is

$$\left[T_N(R) + V(R) + \Delta U(r, R) + \epsilon_k^0(R_0) - E^0_{total} \right] \chi_k(R) = 0 \tag{4.31}$$

Because $\Delta U(r, R)$ depends on both the electronic and nuclear coordinates, (4.31) as written cannot be solved for all values of r.

The Schrodinger equation for the entire system is

$$\left[T_N(R) + V(R) + \Delta U(r, R) + \epsilon_i^0(R_0) - E_{total}^0\right] \sum_i \phi_i^0(r, R)\rangle \chi(R) = 0 \quad (4.32)$$

Operating on (4.27) with $\phi_k^0(r, R_0)\Big|$ we obtain

$$
\begin{aligned}
\langle\phi_k^0(r, R_0)\Big| &\left[T_N(R) + V(R) + \Delta U(r, R) + \epsilon_k^0(R_0) - E_{total}^0\right]\Big| \sum_i \phi_i^0(r, R_0)\rangle \chi_k(R) \\
= &\left\{T_N(R) + V(R) + \epsilon_k^0(R_0) - E_{total}^0 + \langle\phi_k^0(r, R_0)\Big|\Delta U(r, R_0)\Big|\phi_k^0(r, R_0)\rangle\right\} \chi_k(R) \\
&+ \sum_{i\neq k}\langle\phi_k^0(r, R_0)|\Delta U(r, R)|\phi_i^0(r, R_0)\rangle \chi_k(R) = 0
\end{aligned}
$$
$$(4.33)$$

Note that we have separated out the diagonal matrix element of $\Delta U(r, R)$, which does not connect different electronic states. All terms in the brackets {} depend only on R. Also, because R_0 represents fixed coordinates, T_N does not act on the electronic wavefunctions, as it did in the previous two sections.

Neglecting the off-diagonal terms in (4.33), which couple the electronic to the nuclear motion, results in:

$$\left\{T_N(R) + V(R) + \epsilon_k^0(R_0) - E_{total}^0 + \langle\phi_k^0(r, R_0)\Big|\Delta U(r, R)\Big|\phi_k^0(r, R_0)\rangle\right\} \chi_k(R) = 0.$$
$$(4.34)$$

Equation (4.34) can be solved to find the nuclear wavefunctions, $\chi_k(R)$. Finally, the separation of the electronic and nuclear wavefunctions into functions of r and R, respectively, allows the wavefunction of the system to be written as

$$\Psi(r, R) = \phi_k^0(r, R)\chi_k(R) \quad (4.35)$$

Of course, the $\chi_k(R)$ in (4.35) are different from those in (4.17) and (4.27). Equations (4.29), (4.30) and (4.35) define the *Crude Adiabatic Approximation*. The defining characteristic of this approximation is that the electronic wavefunction are determined with the nuclei fixed at fixed positions.

In each of the three forms of the adiabatic approximations presented, the total wavefunction is a product of an electronic wavefunction and a nuclear wavefunction, thus separating the fast and slow subsystems. The next section is devoted to finding expressions for the coupling between the electronic and nuclear subsystems, known as the electron-phonon coupling. Before proceeding, we make the following observations.

1. In deriving the Crude Adiabatic Approximation, we neglected the off diagonal matrix elements between electronic states of the potential energy term in the Hamiltonian, $\Delta U(r, R)$. On the other hand, in the adiabatic approximation in

Sects. 4.2.2 and 4.2.3, the neglected terms arose from the kinetic energy term, T_N, operating on the electronic wavefunctions. Thus, the different formalisms presented in the previous sections neglect different terms in the Hamiltonian in order to separate the fast and slow subsystems. It should not be surprising, then, that these different formalisms will give rise to different forms for the electron-phonon coupling.

2. The Crude Adiabatic Approximation assumes that the positions of the nuclei are fixed. If we take this position to be that at which the ground state of the ion is at equilibrium, this approximation is only valid in systems for which the higher electronic states have equilibrium positions close to that of the ground state. Such is the case for ions in electronic states that are weakly coupled to the lattice. Examples are the 4f states of the lanthanides ions and also the ^2E level of the Cr^{3+}.

3. The neglected terms in the Born-Oppenheimer and Born-Huang Adiabatic Approximations are valid starting points for finding the electron-phonon coupling in weakly- and strongly-coupled systems. Transitions among most *d*-states in transition metal ions and *f-f* or *f-d* transition in rare earth ions can be treated with electron-phonon couplings found from the neglected terms in the Born-Oppenheimer or Born-Huang formalisms.

4.4 Electron-Phonon Coupling

A breakdown in the adiabatic approximation leads to an interaction that couples the electronic motion to the nuclear motion, allowing from the conversion of electron energy to be converted into the kinetic and potential energy associated with of the vibration of the nuclei. This interaction is often called the electron-phonon interaction, and is formally included in the quantum mechanical transition matrix elements as an electron-phonon coupling operator. In this section, we present the two most commonly used expressions for the electron-phonon coupling operator for an ion in a solid. These operators are used to explain a variety of phonon-related transitions between different electronic states, including vibronic absorption and emission, one-phonon transitions, multiphonon relaxation, and Raman scattering.

4.4.1 Type A Electron-Phonon Coupling

In the Crude Adiabatic Approximation, we neglected the off-diagonal terms of $\Delta U(r, R)$, which takes into account the change in potential energy of the system due to the motion of the nuclei. To find the electron-phonon coupling within this approximation, we first write $\Delta U(r, R)$ in a more useful form.

In the presence of an acoustic wave, the optically active ion is displaced from its equilibrium positions, changing the energy of the system. This change in energy is due only to a *relative* change in the distance between the optically active ion and its neighbors. We denote the distance between the optically active ion and its neighbor (labeled α) as $R_{ion,\alpha}$, and the equilibrium distance between them as $R_{ion,\alpha,0}$. For the systems considered in this work, the wavefunctions are highly localized to the central ion, and so we need concern ourselves mainly with the perturbation of the optically active ion by the motion of the surrounding ions. The change in the potential energy between the optically active ion and its neighbors due to the vibrations, which we write as $\Delta U_{ion}(r,R)$, can be expressed in terms of a Taylor expansion:

$$\Delta U_{ion}(r,R) = U_{ion}(r,R) - U_{ion}(r,R_0)$$
$$= \sum_{\alpha} \left[\frac{\partial U_{ion}}{\partial R_{\alpha}} \right]_0 (R_{ion,\alpha} - R_{ion,\alpha,0}) +$$
$$\frac{1}{2} \sum_{\alpha,\beta} \left[\frac{\partial^2 U_{ion}}{\partial R_{ion,\beta} \partial R_{ion,\alpha}} \right]_0 (R_{ion,\alpha} - R_{ion,\alpha,0})(R_{ion,\alpha} - R_{ion,\beta,0}) + \cdots$$
$$= \Delta U_{ion}^{(1)} + \Delta U_{ion}^{(2)} + \cdots$$
(4.36)

where $\Delta U_{ion}^{(1)}$ and $\Delta U_{ion}^{(2)}$ are given by

$$\Delta U_{ion}^{(1)} = \sum_{\alpha} \left[\frac{\partial U_{ion}}{\partial R_{\alpha}} \right]_0 (R_{ion,\alpha} - R_{ion,\alpha,0}) \tag{4.37}$$

$$\Delta U_{ion}^{(2)} = \frac{1}{2} \sum_{\alpha,\beta} \left[\frac{\partial^2 U_{ion}}{\partial R_{ion,\beta} \partial R_{ion,\alpha}} \right]_0 (R_{ion,\alpha} - R_{ion,\alpha,0})(R_{ion,\alpha} - R_{ion,\beta,0}) + \cdots \tag{4.38}$$

In order to gain physical insight into these terms, we consider the simple case of a linear solid, shown in Fig. 4.3. The atoms nuclei are separated from their neighbors by a distance a, and they are free to vibrate longitudinally. The displacement of the *lth* ion from its equilibrium position is given by q_l. In addition to the displacements, Fig. 4.3 also shows a representation of the acoustic wave in the crystal. In the long wavelength approximation, the strain, ε_l, at the *lth* site can be written as [4]:

$$\varepsilon_l = \frac{\partial q_l}{\partial x} \approx \frac{q_{l+1} - q_l}{a} = \frac{(x_{l+1} - x_l) - a}{a}. \tag{4.39}$$

Thus, the strain is proportional to the change in distance between the optically active ion and a neighboring ion. In the case of an ion in a solid, $(x_{l+1} - x_l) - a$ in (4.39) is replaced by $R_{ion,\alpha} - R_{ion,\alpha,0}$. Comparing (4.39) and (4.36),
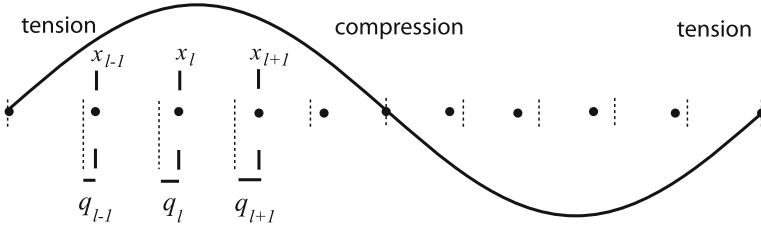
Fig. 4.3 Representation of a one-dimensional solid in the presence of a longitudinal acoustic wave. Equilibrium positions of the atoms are given by the dashed lines, separated by a distance a, and actual positions are labeled by x_l. The sine wave is a representation of the displacement of the ions from equilibrium as a function of the horizontal position, with regions of tension and compression indicated. In the long wavelength approximation, the strain in the lattice is proportional to $(q_{l+1} - q_l)$ (Figure 4.3 is adapted from Ref. [4])

the change in potential energy experienced by the optically active ion due to the displacements of the ions in the solid can be written as the sum of powers of the strain.

$$\Delta U_{ion}(r, R) = \sum_{\alpha} V_{1,\alpha} \varepsilon_{\alpha} + \sum_{\alpha} V_{2,\alpha} \varepsilon_{\alpha}^2 + \cdots \tag{4.40}$$

For a linear system of like ions experiencing a longitudinal wave, as shown in Fig. 4.3, the form of the strain given in (4.39) is particularly simple. For a three dimensional crystal consisting of different ion types, transverse and longitudinal waves, and going beyond the long wavelength limit, the situation is very much more complex. We shall, however, make the assumption that we can write the $\Delta U_{ion}(r, R)$ in the form given in (4.40). We will utilize Eq. (4.40) later in this paper.

In a perturbation treatment, the first term given in (4.36) can be used to find the first order correction to the electronic wavefunction:

$$\phi_i(r, R) = \phi_i^0(r, R_0) + \sum_{j \neq i} \frac{\left\langle \phi_j(r, R_0) \left| \Delta U_{ion}^{(1)} \right| \phi_i(r, R_0) \right\rangle}{\epsilon_j - \epsilon_i} \phi_j(r, R_0) \tag{4.41}$$

The states in the Crude Adiabatic Approximation corrected to the first order are:

$$\Psi_{i,k}^{(1)}(r, R) = \left[\phi_i^0(r, R_0) + \sum_{j \neq i} \frac{\left\langle \phi_j(r, R_0) \left| \Delta U_{ion}^{(1)} \right| \phi_i(r, R_0) \right\rangle}{\epsilon_j - \epsilon_i} \phi_i(r, R_0) \right] \chi_k(R)$$
$$\tag{4.42}$$

The sum in (4.42) contains terms of the form $\left\langle \phi_j(r, R_0) \left| \Delta U_{ion}^{(1)} \right| \phi_i(r, R_0) \right\rangle$, which mix the various electronic states of the system, indicating that the displacements of the nuclei from equilibrium cause transitions from one electronic state to

another. Thus, $\Delta U_{ion}^{(1)}$ is an example of an electron-phonon coupling operator. It is interesting to note that the wavefunctions in (4.42) are the product of a purely electronic wavefunction, in brackets [], with nuclear wavefunction. That is, when $\Delta U_{ion}^{(1)}$ is used as a perturbation to the electronic wavefunction only, it mixes various electronic states, but does not couple the electronic wavefunction to the vibrational wavefunction. The electronic and the nuclear states are not truly coupled in the usual sense, and the corrected wavefunction (4.42) is still considered "adiabatic". This type of the coupling is known as *electron-phonon coupling of type A* [6].

4.4.2 Type B Electron-Phonon Coupling

In the Born Oppenheimer Adiabatic Approximation (Sect. 4.2.2), the states of the system are given by (4.27). We define a non-adiabatic Hamiltonian, H_{NA}, by the neglected, off-diagonal matrix elements of the last two terms in (4.15) in the following manner.

$$
\begin{aligned}
H_{NA}\Psi_{i,k}(r,R) = &-\frac{\hbar^2}{2}\sum_k\sum_\alpha\frac{1}{M_\alpha}\chi_{i,k}(R)\overrightarrow{\nabla}_\alpha^2\phi_i(r,R) \\
&-\hbar^2\sum_k\sum_\alpha\frac{1}{M_\alpha}\left(\overrightarrow{\nabla}_\alpha\phi_i(r,R)\right)\cdot\left(\overrightarrow{\nabla}_\alpha\chi_{i,k}(R)\right)
\end{aligned}
\tag{4.43}
$$

At this point, it is typical to assume that the first term on the right in (4.43) is negligible compared with the second. Under that assumption, (4.38) becomes

$$
H'_{NA}\Psi_{i,k}(r,R) = -\hbar^2\sum_k\sum_\alpha\frac{1}{M_\alpha}\left(\overrightarrow{\nabla}_\alpha\phi_i(r,R)\right)\cdot\left(\overrightarrow{\nabla}_\alpha\chi_{i,k}\right).
\tag{4.44}
$$

Treating H'_{NA} as a perturbation, the first order, non-adiabatic wavefunction is given by:

$$
\begin{aligned}
\Psi_{i,k}^{(1)}(r,R) = \Psi_{i,k}(r,R) - \sum_{j\neq i}\sum_\alpha\frac{\hbar^2}{M_\alpha}\frac{\left\langle\Psi_{j,k}(r,R)\left|\left(\overrightarrow{\nabla}_\alpha\phi_i(r,R)\right)\cdot\left(\overrightarrow{\nabla}_\alpha\chi_{i,k}\right)\right|\Psi_k(r,R)\right\rangle}{E_j-E_i} \\
\times\Psi_{j,k}(r,R)
\end{aligned}
\tag{4.45}
$$

The wavefunction $\Psi_{i,k}^{(1)}$ in (4.45) cannot be expressed as a product of an electronic wavefunction and a nuclear wavefunction, so it is a true non-adiabatic wavefunction. The electron-phonon coupling operator expressed in (4.44) leads to a breakdown of the adiabatic approximation, coupling the electronic and nuclear motions and

allowing the nuclear motion to cause transitions between electronic states. H'_{NA} is sometimes referred to as the *electron-phonon coupling of type B*[6].

4.5 Representation of Eigenstates and Operators

In order to apply the previous treatments to phonon-related processes in solids, we must first represent the vibrational states of the lattice and electron-phonon coupling operators in the appropriate forms. To do so, we make the following assumptions:

1. *The nuclei vibrate in a harmonic potential.* In this so-called "harmonic approximation", each normal coordinates Q_k, is associated with the *kth* vibrational mode of the solid and oscillates with a frequency ω_k. Each mode acts as a harmonic oscillator, with the excitation of the *kth* oscillator corresponding to the number of phonons, n_k, in that mode. The energy of the lattice is:

$$E = E_0 + \sum_k \left(n_k + \frac{1}{2} \right) \hbar \omega_k \qquad (4.46)$$

where E_0 is the energy of the lattice with the nuclei at their equilibrium positions.

2. *The normal modes of the solid act independently, with no communication between them.* In this assumption, the eigenstates of the lattice vibrations, $\chi(Q_k)$, are products of the states of the normal modes:

$$\chi(Q_k) = \prod_k \left| n_k \right\rangle = |n_1\rangle |n_2\rangle |n_3\rangle \dots |n_k\rangle \dots \left| n_{3N-6} \right\rangle, \qquad (4.47)$$

where N is the number of atoms in the solid.

It should be noted that neither of the assumptions above are strictly valid. Experiments on phonon decay times have shown that phonons generally do decay into other, lower energy modes [e.g. 10, 11]. Also, the assumption of a harmonic approximation is only valid for very small amplitudes of vibration. As the amplitudes increase (i.e., as temperature increases), the restoring force becomes more non-linear. Frenkel noted early on that such non-linear effects cause a breakdown of the adiabatic separation between the electronic and nuclear subsystems, thus allowing lattice vibrations to cause electronic transitions [12]. Despite these assumptions, working with the states as described in (4.47) does lead to results that adequately explain the behavior of many systems across a range of temperatures.

In Sect. 4.3 we derived the electron-phonon coupling operators (types A and B) in terms of the nuclear coordinates. Within the constraints of the above assumptions,

we now present the form of those electron-phonon coupling operators in terms of the normal coordinates.

The electron-phonon coupling of type A, in terms of the strain operator, is given in Eq. (4.39). It is convenient to express the strain in terms of the phonon annihilation and creation operators, a and $a^\dagger$, respectively. We do not derive this expression here, but simply present the result. The reader is referred to the text by Henderson and Imbusch [4] for the details of the derivation.

Referring to the example of a linear solid shown in Fig. 4.3, it can be shown that the displacement of the *lth* ion from its equilibrium position, q_l, can be written in terms of the generalized position has the following form [4]:

$$q_l = \left(\frac{1}{N}\right)^{1/2} \sum_k Q_k exp\left(-i\kappa a\right) \tag{4.48}$$

where a is the spacing between atoms, k is the wave vector associated with the *kth* mode, N is the number of atoms in the linear chain. Using (4.48), the local strain at the site of the *lth* ion, as approximated in (4.39), due to the *kth* normal mode can be expressed in terms of a_k and $a_k^\dagger$ as follows:

$$\varepsilon_k = -i\left(\frac{\hbar\omega_k}{2MNv_k^2}\right)^{1/2} \left(a_k^\dagger - a_k\right) \tag{4.49}$$

In (4.49) v_k is the velocity of the sound associated with the *kth* mode. Again, the reader is referred to [4] for the full derivation of (4.49). The operator for the electron-phonon coupling of type A is obtained by inserting (4.49) into the expansion similar to (4.40), except the sum is over all the normal coordinates. Keeping only the first two terms, the result is:

$$\Delta U_{ion} \approx \Delta U_{ion}^{(1)} + \Delta U_{ion}^{(2)} = V_{1,k}\varepsilon_k + V_{2,k}\varepsilon_k^2 \tag{4.50}$$

Recall that (4.48) applies to a linear chain of atoms in the long wavelength approximation. For practical reasons, however, it is usually assumed that the simplified version of the strain operator in (4.49) has the same form for all normal modes in a three-dimensional crystal with different masses, whether those modes correspond to transverse or longitudinal waves.

The electron phonon coupling of type B is given by the non-adiabatic Hamiltonian, H_{NA}', defined by Eq. (4.44). To express (4.44) in terms of the normal coordinates, recall that $i\hbar \vec{\nabla}_\alpha = P_\alpha$. The kinetic energy of the lattice in Cartesian coordinates and in normal coordinates is:

$$T_N = \sum_\alpha \frac{P_\alpha^2}{2M_\alpha} = \sum_k \frac{P_k^2}{2M} = -\hbar^2 \sum_k \frac{1}{2M} \left(\frac{\partial}{\partial Q_k}\right)^2 \tag{4.51}$$

where the first sum is over all nuclei, the second and third sums are over all normal modes, and M is a properly weighted mass. Using the term on the far right in (4.51), and re-deriving Eq. (4.44), it is readily seen that the electron-phonon coupling operator of type B operating on the adiabatic wavefunction of the system is expressed as:

$$H'_{NA}\Psi_i(r, Q) = -\hbar^2 \sum_k \frac{1}{M} \left(\frac{\partial \phi_i(r, Q)}{\partial Q_k} \right) \cdot \left(\frac{\partial \chi_{i,}(Q)}{\partial Q_k} \right) \qquad (4.52)$$

This defines the non-adiabatic operator written in terms of the normal coordinates of the lattice. We note that calculating the first term in parentheses in (4.52) is very difficult, requiring detailed knowledge of the electronic wavefunction. On the other hand, the last term in the sum in (4.52) is readily calculated in the harmonic approximation, since it contains the first derivatives of the standard harmonic oscillator wavefunctions. The matrix elements containing this term are frequently calculated in determining non-radiative transition rates between electronic levels using a single configurational coordinate model [13,14, and references therein].

4.6 Thermal Broadening and Shifting of Sharp Spectral Lines

4.6.1 Thermal Broadening of Spectral Lines

The broadening of a spectral line can be caused by several interactions, among which are the following:

1. Strain Broadening – These are site-to-site variations in the crystalline field at the ion due to strains in the crystal. This is a static interaction and is present at even low temperatures.
2. Lifetime Broadening: This category includes all processes that affect the lifetime (τ) of the ion in its excited state, thereby changing the linewidth (ΔE) through the uncertainty relation: $\Delta E \tau \geq \hbar/2$. The processes are radiative decay, nonradiative decay, and vibronic transitions. Even for allowed transitions, the broadening due to this term is less than the strain broadening observed in single crystals.
3. Direct processes: These processes involve a transition from one level to another via the absorption or emission of a phonon. This term has been found to be of secondary importance in most systems, and so will not be discussed here.
4. Raman Scattering: This occurs via the emission of a phonon at one frequency and the absorption of another phonon at a different frequency, and where the initial and final electronic states are the same, and the intermediate state is virtual. It is a second order process, and is found to be the dominant contributor to the shift in several systems [e.g. 15–18]. This process is shown in Fig. 4.4.
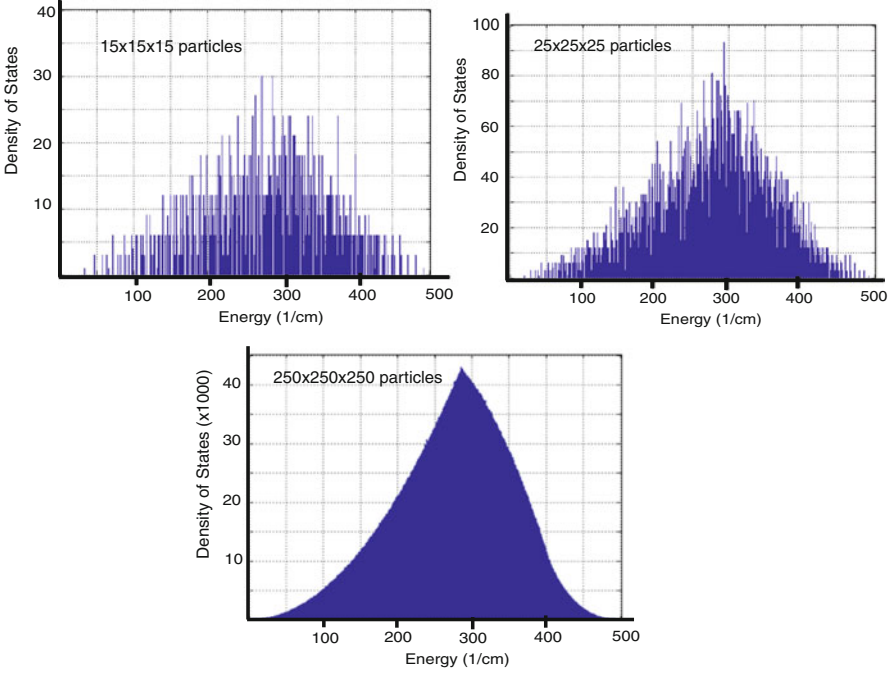
Fig. 4.4 The phonon density of states vs. phonon energy of cubic nanoparticles with (*left*) $15 \times 15 \times 15$ atoms, (*center*) $25 \times 25 \times 25$ atoms, and (*bottom*)$250 \times 250 \times 250$ atoms. The velocity of sound was set to 3400 m/s

To investigate this interaction, we utilize the electron-phonon coupling of type A, as given by Eqs. (4.49) and (4.50). For weak electron-phonon coupling, Eqs. (4.49) and (4.50) can be used to determine the interaction term to the second order. The result is:

$$\Delta U_{ion} \approx \Delta U_{ion}^{(1)} + \Delta U_{ion}^{(2)}$$

$$= V_1 \sum_k \left(\frac{\hbar \omega_k}{2Mv^2}\right)^{1/2} \left(a_k - a_k^\dagger\right) + V_2 \frac{\hbar}{2Mv^2} \sum_k \sqrt{\omega_k \omega_{k'}} \left(a_k - a_k^\dagger\right) \left(a_{k'} - a_{k'}^\dagger\right). \tag{4.53}$$

where we have assumed V_1 and V_2 are independent of the phonon mode k. The states of the system are products of an electronic part and a nuclear part.

$$|\Psi\rangle = |\phi\rangle \otimes |n_1 n_2 n_3 \ldots n_k \ldots\rangle = |\phi, n_1 n_2 n_3 \ldots n_k \ldots\rangle \tag{4.54}$$

Since Raman scattering is a second order process, the contributing terms derive from: (4.1) the first order term in (4.53) with the first order correction to the initial

and final states, and (4.2) the second order term in (4.5) with the zeroth order states. The relevant matrix element for the Raman process is:

$$
\begin{aligned}
&\left\langle \Psi_f \middle| \Delta U_{ion} \middle| \Psi_i \right\rangle \\
&= \sum_j \frac{\left\langle \phi_i^0, n_k-1, n_{k'}+1 \middle| \Delta U_{ion}^{(1)} \middle| \phi_j^0 n_k-1, n_{k'} \right\rangle \left\langle \phi_j^0, n_k-1, n_{k'} \middle| \Delta U_{ion}^{(1)} \middle| \phi_i^0, n_k, n_{k'} \right\rangle}{\epsilon_i - \left(\epsilon_j - \hbar\omega_k \right)} \\
&+ \sum_j \frac{\left\langle \phi_i^0, n_k-1, n_{k'}+1 \middle| \Delta U_{ion}^{(1)} \middle| \phi_j^0 n_k-1, n_{k'} \right\rangle \left\langle \phi_j^0, n_k, n_{k'}+1 \middle| \Delta U_{ion}^{(1)} \middle| \phi_i^0, n_k, n_{k'} \right\rangle}{\epsilon_i - \left(\epsilon_j - \hbar\omega_{k'} \right)} \\
&+ \left\langle \phi_i^0, n_k-1, n_{k'}+1 \middle| \Delta U_{ion}^{(2)} \middle| \phi_i^0, n_k, n_{k'} \right\rangle
\end{aligned}
\tag{4.55}
$$

Using (4.53) to replace for $\Delta U_{ion}^{(1)}$ and $\Delta U_{ion}^{(2)}$ in (4.55), recalling that $a \left| n \right\rangle = \sqrt{n} \left| n-1 \right\rangle$ and $a^\dagger \left| n \right\rangle = \sqrt{n+1} \left| n+1 \right\rangle$, and assuming that $\omega_k, \omega_{k'} \ll \epsilon_j$ for all intermediate states, j, (4.55) becomes:

$$
\left\langle \Psi_f \middle| \Delta U_{ion} \middle| \Psi_i \right\rangle = \alpha' \sqrt{\omega_k \omega_{k'} n_k \left(n_{k'} + 1 \right)}
\tag{4.56}
$$

where

$$
\alpha' = \frac{\hbar}{Mv^2} \left[\sum_{j \neq i} \frac{\left| \left\langle \phi_j \middle| V_1 \middle| \phi_i \right\rangle \right|^2}{\epsilon_i - \epsilon_j} + \left\langle \phi_i \middle| V_2 \middle| \phi_i \right\rangle \right].
\tag{4.57}
$$

The transition probability per unit time due to modes k and k' is

$$
\left(W_{Raman} \right)_{kk'} = \frac{2\pi}{\hbar^2} \left| \alpha' \right|^2 \omega_k \omega_{k'} n_k \left(n_{k'} + 1 \right) \varrho \left(\omega_f \right),
\tag{4.58}
$$

where $\varrho(\omega_f)$ represents the density of final states of the phonon field. To find the total transition rate for these Raman processes, we must integrate over all phonon modes k and k'. For sharp lines, where the width of the line is much less than the Debye frequency, we estimate $\varrho(\omega_f)$ as

$$
\varrho \left(\omega_f \right) \simeq \varrho \left(\omega_k \right) \varrho \left(\omega_{k'} \right) \delta \left(\omega_k - \omega_{k'} \right) d\omega_k d\omega_{k'} = \varrho^2 \left(\omega_k \right) d\omega_k.
\tag{4.59}
$$

Inserting (4.59) into (4.58) and integrating over all phonon modes, we obtain:

$$W_{Raman} = \frac{2\pi}{\hbar^2} \left| \alpha' \right|^2 \int \omega_k^2 n_k \left(n_k + 1 \right) \varrho^2 \left(\omega_k \right) d\omega_k \tag{4.60}$$

Recalling the expression for the phonon occupation number of the *kth* mode,

$$n_k = \frac{1}{e^{\hbar \omega_k / kT} - 1}, \tag{4.61}$$

the total transition probability becomes

$$W_{Raman} = \frac{2\pi}{\hbar^2} \left| \alpha' \right|^2 \int \omega_k^2 \varrho^2 \left(\omega_k \right) \frac{e^{\hbar \omega_k / kT}}{\left(e^{\hbar \omega_k / kT} - 1 \right)^2} d\omega_k . \tag{4.62}$$

In the Debye approximation, $\varrho(\omega) = 3V\omega^2 / 2\pi^2 v_s^3$, (4.61) takes the following form:

$$W_{Raman} = \frac{2\pi}{\hbar^2} \left| \alpha' \right|^2 \frac{9V^2}{4\pi^4 v_s^6} \int_0^{\omega_D} \frac{\omega_k^6 \, e^{\hbar \omega / kT}}{\left(e^{\hbar \omega_k / kT} - 1 \right)^2} d\omega_k, \tag{4.63}$$

where ω_D is the Debye frequency. It is convenient to rewrite (4.63) in terms of the unitless parameter $x = \hbar\omega / kT$ and the Debye temperature $T_D = \hbar\omega_D$. The result is:

$$W_{Raman} = \overline{\alpha} \left(\frac{T}{T_D} \right)^7 \int_0^{T_D / T} \frac{x^6 e^x}{(e^x - 1)^2} dx . \tag{4.64}$$

where $\overline{\alpha} = \frac{9V^2}{2\pi\hbar^2} \left(\frac{\omega_D}{v_s} \right)^6 \left| \alpha' \right|^2$, and is referred to as the electron-phonon coupling constant.

The temperature dependence of (4.64) is contained in the T^7 term outside the integral and in the upper limit of the integral, T_D/T. In the limit as $T \to 0$, the upper limit goes to infinity, and the integral is simply a constant, so the contribution of Raman processes to the linewidth goes as T^7, which goes to zero as $T \to 0$. At $T \gg T_D$ we may use the approximation $e^x \sim 1 + x$, so the integral goes roughly as x^5, and the (4.64) goes as T^2.

4.6.2   Thermal Shifting of Spectral Lines

Any interaction of a system an external agent will, in general, affect the energies of the states of the system. As temperature increases, the interaction of the phonons with the electrons also increases, leading to the thermal shift of the energy level. The contribution of the electron-phonon interaction is a second-order effect, and so contains the matrix element of $\Delta U_{ion}^{(2)}$ between the zeroth order states, and of $\Delta U_{ion}^{(1)}$

between the first order states. The correction to the energy of the level due to the electron-phonon interaction is given by:

$$
\begin{aligned}
\Delta\epsilon_{i,k} = {}& \left\langle \phi_i^0,\, n_k \,\middle|\, \Delta U_{ion}^{(2)} \middle|\, \phi_i^0,\, n_k \right\rangle \\
&+ \sum_j \frac{\left\langle \phi_i^0,\, n_k \,\middle|\, \Delta U_{ion}^{(1)} \middle|\, \phi_j^0,\, n_k - 1 \right\rangle \left\langle \phi_j^0,\, n_k - 1 \,\middle|\, \Delta U_{ion}^{(1)} \middle|\, \phi_i^0, n_k \right\rangle}{\epsilon_i - (\epsilon_j - \hbar\omega_{k'})} \\
&+ \sum_j \frac{\left\langle \phi_i^0, n_k \middle| \Delta U_{ion}^{(1)} \middle| \phi_j^0, n_k + 1 \right\rangle \left\langle \phi_{j}, n_k + 1 \middle| \Delta U_{ion}^{(1)} \middle| \phi_i^0, n_k \right\rangle}{\epsilon_i - (\epsilon_j + \hbar\omega_k)}
\end{aligned}
\tag{4.65}
$$

Using (4.53) to rewrite $\Delta U_{ion}^{(1)}$ and $\Delta U_{ion}^{(2)}$ in terms of the creation and annihilation operators, assuming that $\left|\epsilon_i - \epsilon_j\right| \gg \hbar\omega_k$, and using the identities $a\left|n\right\rangle = \sqrt{n}\left|n-1\right\rangle$ and $a^\dagger\left|n\right\rangle = \sqrt{n+1}\left|n+1\right\rangle$, (4.65) reduces to

$$
\Delta\epsilon_{i,k} = \frac{\hbar}{Mv_s^2}\left[\left\langle \phi_i^0\middle|V_2\,\middle|\phi_i^0\right\rangle + \sum_j \frac{\left|\left\langle\phi_i^0\middle|V_1\,\middle|\phi_j^0\right\rangle\right|^2}{\epsilon_i - \epsilon_j}\right]\omega_k\left(2n_k + 1\right)
\tag{4.66}
$$

The thermal shift of the line is due only to the terms containing n_k. The total thermal shift is found by summing over all k. For *large particles*, this sum can be approximated by an integral, so the total shift is given by:

$$
\Delta\epsilon_i = \frac{\hbar}{Mv_s^2}\left[\left\langle\phi_i^0\middle|V_2\,\middle|\phi_i^0\right\rangle + \sum_j \frac{\left|\left\langle\phi_i^0\middle|V_1\,\middle|\phi_j^0\right\rangle\right|^2}{\epsilon_i - \epsilon_j}\right] 2\int \rho\left(\omega_k\right)\omega_k n_k d\omega_k
\tag{4.67}
$$

Assuming the Debye distribution ($\varrho\left(\omega\right) = 3V\omega^2/2\pi^2 v_s^3$), using the equilibrium value of n_k as defined in (4.61), setting the upper limit of the integral in (4.67) to the Debye frequency, and making the substitution $x = \hbar\omega/kT$, the thermal shift of a an energy level becomes:

$$
\delta E_{ther} = \Delta V \int_0^{T_D/T} \frac{x^3}{e^x - 1} dx
\tag{4.68}
$$

where

$$
\Delta V = \frac{2\hbar}{Mv_s^2}\left(\frac{kT}{\hbar}\right)^4\left[\left\langle\phi_i^0\left|V_2\right|\phi_i^0\right\rangle + \sum_j \frac{\left\langle\phi_i^0\left|V_1\right|\phi_j^0\right\rangle^2}{\epsilon_i - \epsilon_j}\right]
\tag{4.69}
$$

The temperature dependence of the thermal shift of a spectral line is determined by the T^4 term contained in ΔV and by the upper limit of the integral. As $T \rightarrow 0$, the integral approaches a constant value, and the line shift goes as T^4. At high T the integrand goes roughly as x^2, the integral goes as T^{-3}, and so the line shift becomes linear with T.
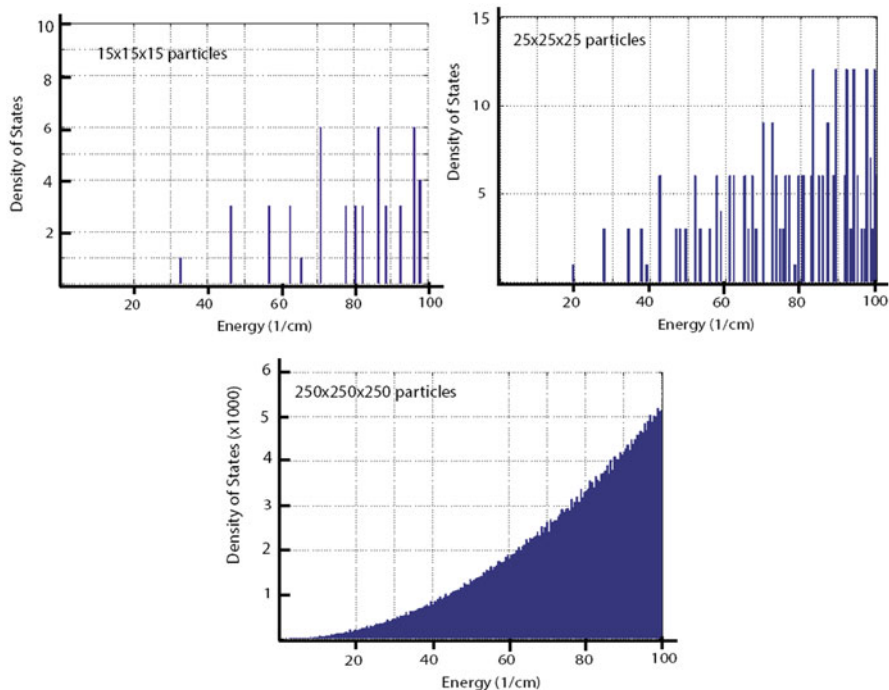
4.7   The Phonon Density of States in Nanoparticles

Consider a simple cubic solid with side length L and atomic spacing a. The wavelengths of the phonons vary from roughly twice the atomic spacing to twice the side length of the particle. The energy of a phonon in such a solid is given by

$$\varepsilon_{ph} = \frac{hv_s}{\lambda} = \frac{hv_s}{2L}n, \tag{4.70}$$

where v_s is the velocity of sound, $n = \left(n_x^2 + n_y^2 + n_z^2\right)^{1/2}$, and n_x, n_y, n_z are integers ranging from 1 to L/a. Note that the maximum phonon energy is determined by the interatomic spacing, and so is independent of the particle size, while the low frequency phonons increase in energy as the particle size, L, decreases. Thus, many low frequency phonons that exist in the bulk are no longer supported in a nanoparticle.

Calculated phonon densities of states (DOS) of cubic nanoparticles $15 \times 15 \times 15$ atoms on a side (L $\sim$ 3 nm), $25 \times 25 \times 25$ atoms on a side (L $\sim$ 5 nm), and that of a nanoparticle $250 \times 250 \times 250$ atoms on a side (L $\sim$ 50 nm) have been calculated using the speed of sound equal to 3400 m/s and an interatomic spacing of 0.2 nm. The modes were accumulated in 1000 bins, which for the diagrams show were each approximately 0.5 cm^{-1} in width. The results are shown in Fig. 4.4. We note the following:

1. For the $250 \times 250 \times 250$ atoms system, the DOS exhibits a ε^2 dependence, as expected from the Debye theory, out to a frequency at which the DOS reaches a maximum. At higher energies, the DOS is decidedly un-Debye-like, decreasing smoothly to zero. This behavior is due to the finite size of the crystal.
2. For the smaller particles, the DOS is a discrete function at lower energies, with a large energy gap between zero energy and the first mode. For 250 nm particles, the DOS appears nearly continuous at all energies, and is very similar in appearance to the DOS in a bulk cubic particle. Figure 4.5, shows the DOS at low phonon energies.
3. The results in Figs. 4.4 and 4.5 are for cubic crystals, but the discreteness of the DOS at low energies is a common feature to all very small particles. The exact shape of the DOS function, however, depends on the particle shape.

Fig. 4.5 The phonon density of states shown in Fig. 4.4 in the energy range from 0 to 100 cm^{-1}

The discreteness seen in the small particle is due to the fact that in going from bulk to nano, the total number of phonon modes decreases drastically. This decrease can be shown by noting that the total number of phonon modes is simply *3 N-6*, where N is the number of atoms in the particle, and can be estimated as $N \sim \left(\frac{L}{a}\right)^3$. For a bulk crystal with $L = 0.3$ cm and $a = 0.2$ nm, $3 N \sim 4.5 \times 10^{21}$, whereas when $L = 3$ nm, $3 N \sim 4.5 \times 10^3$. Thus, going from a particle size of 0.3 cm to 3 nm the total number of allowed phonon modes decreases by 18 orders of magnitude! As a result, the phonon spectrum is no longer a continuous function of energy.

Given the importance that phonon-related processes play in the luminescence behavior of ions in solids, the change in the phonon DOS as one moves from the bulk to the nano regime is likely have observable experimental effects. In the following sections, we take note of experiments that have, and in some cases have not, revealed such effects.

4.8 Effect of the Phonon DOS on the Establishment of Thermal Equilibrium

Following absorption of a photon, a luminescent ion generally relaxes to a state of quasi-thermal equilibrium. The time it takes to reach this quasi-thermal equilibrium is generally on the order of picoseconds. The relaxation can be within a single electronic state or among different electronic states, the latter of which would require the breakdown of the adiabatic approximation. Even relaxation within the same electronic state requires the participation of all phonon modes and the mixing of those modes for thermal equilibrium to be established. For small particles, where the low frequency modes are discrete and well separated from one another, we may expect the establishment thermal equilibrium following excitation to be inhibited.

Experimental evidence of this effect has been observed by G. Liu et al. [19, 20], who conducted emission and excitation experiments on nanoparticles of Er-doped Y_2O_3 with radii of $\sim$400 nm and 25 nm. Figure 4.6 shows an emission spectrum at 3 K of the $^4S_{3/2} \rightarrow {}^4I_{11/2}$ transition of Er in Y_2O_3 following excitation with a pulsed laser at energy levels into the $^4F_{7/2}$ manifold. In the 400 nm particles, the emission originates from only the lowest energy level of the $^4S_{3/2}$ manifold. In the 25 nm nanoparticles, however, anomalous hot emission bands are observed. Excitation into
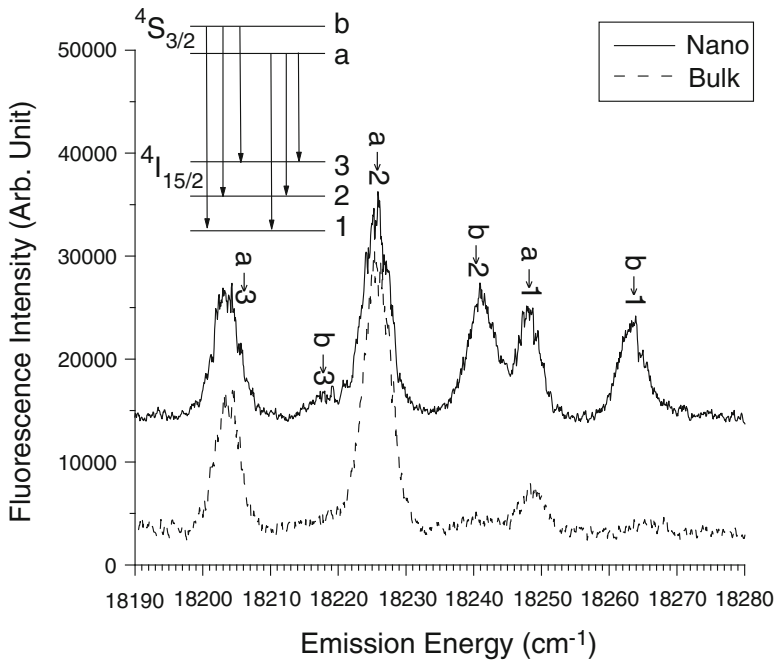
Fig. 4.6 The luminescence of the $^4S_{3/2}$ to $^4I_{15/2}$ transition in bulk (*dotted line*) and diameter nanocrystals (*solid line*) of Er:Y_2O_2S at 2.6 K [19]

the $^4F_{7/2}$ levels is followed by fast relaxation to the $^4S_{3/2}$, resulting in the population of the upper crystal field level of that manifold. In the 400 nm particles there is fast relaxation from level (b) of the $^4S_{3/2}$ manifold to its lower level (a) (See Fig. 4.6). In the 25 nm particles, however, there is no available mode to accept a phonon of that low frequency ($\sim$25 cm^{-1}). Consequently, the one-phonon decay process at that energy does not occur in the nanoparticle, and level (b) remains populated long enough to emit a photon.

This experiment demonstrates the effect of the discreteness of the phonon DOS in small particles. However, it also hints that observing such effects may be difficult; the discreteness of the phonon DOS can be masked by second-order processes and/or by the mixing of phonons due to anharmonic contributions to the potential, even at low temperatures.

4.9 Thermal Broadening and Shifting of Sharp Spectral Lines in Nanoparticles

In this section, we focus on the changes in the density of states of nanoparticles of different sizes affects the shift thermal broadening and shifting of sharp spectral lines.

4.9.1 Broadening of a Spectral Line in a Nanoparticle

In Sect. 4.6, the broadening of a spectral line was found to depend on the density of phonon states and on the phonon occupation number of each state. Earlier, we estimated the phonon density of states using Debye approximation, and the sum over all phonon states was carried out by integration. For nanoparticles, the density of phonon states is a discrete function, and the sum over states can be carried out directly. We begin our discussion of the thermal broadening of a spectral line in a nanoparticle with Eq. (4.58):

$$(W_{Raman})_{kk'} = \frac{2\pi}{\hbar^2} |\alpha'|^2 \omega_k \omega_{k'} n_k (n_{k'} + 1) \varrho (\omega_f), \qquad (4.71)$$

where α' is given by (4.57).

The total transition rate is found by summing over all final states of the lattice, subject to the condition that energy must be conserved. In nanoparticles, the density of phonon states, $\varrho_{nano}(\omega)$, depends on the size and shape of the sample. Examples are shown in Fig. 4.4. In describing the density of phonon states, it is important to recall that each phonon mode represents a resonance peak with a particular line shape ($f(\omega)$) and line width ($\Delta\omega$). The density of states may be written as:

$$\varrho_{nano}(\omega_i) = g(\omega_i)f(\omega_i) \qquad (4.72)$$

where $g(\omega_i)$ is the degeneracy modes at frequency ω_i. Though the line shape is more correctly represented as a Lorentzian, we shall simplify the shape to the "top hat" function, that is:

$$f(\omega) = \begin{cases} 1/\Delta\omega \text{ for } \omega - \Delta\omega \leq \omega \leq \omega + \Delta\omega \\ 0 \text{ elsewhere} \end{cases} \qquad (4.73)$$

We also assume that line width of each resonance is $\Delta\omega$, independent of ω. For sharp spectral lines, we further assume that the main contribution to the broadening occurs when $|\omega_k - \omega_{k'}| \leq \Delta\omega/2$, that is, the phonons in the scattering process are of nearly the same frequency. In such a scheme, we may approximate the density of final states as

$$\varrho(\omega_f) = \varrho_{nano}(\omega_i)\varrho_{nano}(\omega_i')\Delta\omega\Delta\omega'\delta(\omega_i - \omega_i') \qquad (4.74)$$

Summing (4.71) over phonon frequencies, and using (4.72), (4.73) and (4.74), the total transition rate of the Raman process is

$$W_{Raman} = \frac{2\pi}{\hbar^2}|\alpha'|^2\sum_i g^2(\omega_i)\omega_i^2 n_{\omega_i}(n_{\omega_i} + 1)f^2(\omega)\Delta\omega$$

$$= \frac{2\pi}{\hbar^2}|\alpha'|^2\frac{1}{\Delta\omega}\sum_i g^2(\omega_i)\omega_i^2 n_{\omega_i}(n_{\omega_i} + 1) \qquad (4.75)$$

The degeneracy term $g(\omega)$ includes all modes within a range $\omega \pm \Delta\omega/2$. In Fig. 4.4, the energy axes are broken up into 1000 bins, each of energy ~ 0.5 cm^{-1}. $g(\omega_i)$ is given by the number of modes in the ith bin, where ω_i is the central frequency of the bin. The sum in (4.78), which carries the temperature dependence of the broadening, was carried out for four particle sizes from T=1 K to T=700 K. The results are shown in Fig. 4.7.

We make the following observations regarding these results.

1. The strongest temperature dependence of the line broadening for all particle sizes occurs at temperatures below 10 K. For the 3 nm ($15 \times 15 \times 15$ atoms) nanoparticle, the temperature dependence is strong between 1 K and 10 K.
2. Above 300 K the curvature of the lines in Fig. 4.7 are independent of particle size, thus thermal dependence of the broadening should be the same for particles of all sizes.
3. Figure 4.7 also shows that above ~ 10 K the expected broadening to be larger for smaller particle sizes. However, this effect depends on the details of the calculation (e.g. the binning of the data and the "top hat" line shape function), and should not be taken too seriously.

To understand the strong temperature dependence of the broadening at low temperatures, it is useful to consider not just the phonon density of states, but also

the phonon occupancies. Figure 4.8 shows the product $\varrho_{nano}(\epsilon)n(\epsilon)$ for the 3 nm particle at T = 10 K, 100 K, and 500 K. At 10 K, only a few modes are occupied, and even then the phonon occupation numbers are very small, much less than 1. At 1 K, the occupancy of the lowest mode in the 3 nm particle is $\sim 10^{-23}$. Thus, in a nanoparticle there are essentially no phonons at 1 K, so there is no broadening. This helps explain the steep slope for the 3 nm particle in Fig. 4.7 at temperatures less that a few degrees K.

Using hole-burning experiments, Meltzer and Hong [21] examined the broadening of the $^7F_0 \rightarrow {}^5D_0$ transition of Eu_2O_3 spherical nanoparticles of different diameters (5.4, 7.6, and 11.6 nm) at temperatures between 4 K and 10 K. They observed a T^n dependence, where $3 < n < 4$, for the thermal broadening of the line. This dependence is much smaller than that shown in Fig. 4.7 for the 5 nm particles, and was also much smaller than their own calculated predictions. In contradiction to the results in Fig. 4.7, the authors observed the thermal broadening increasing as the particle size decreases. To explain this they refer to calculations that posit an inverse relation between the electron-phonon coupling and particle size [22].

Erdem et al. [23] measured the linewidth of the $^2E \rightarrow {}^4T_2$ transition of Cr-doped YAG nanoparticles at temperatures from 30 K to 300 K as a function of particle size (Fig. 4.9). The results were fit to Eq. (4.64) assuming Debye temperature of 550 K and where the electron-phonon coupling parameter, α', was allowed to vary. The fits to Eq. (4.64) are reasonably good, showing that even in nanoparticles as small as 28 nm behave similar to the bulk crystal. This is consistent with the behavior shown in Fig. 4.7. Excellent fits to Eq. (4.64) were also reported by Bilir et al. on the temperature dependence of the linewidth of Nd nanoparticles ranging in diameters from 16 to 250 nm [24].
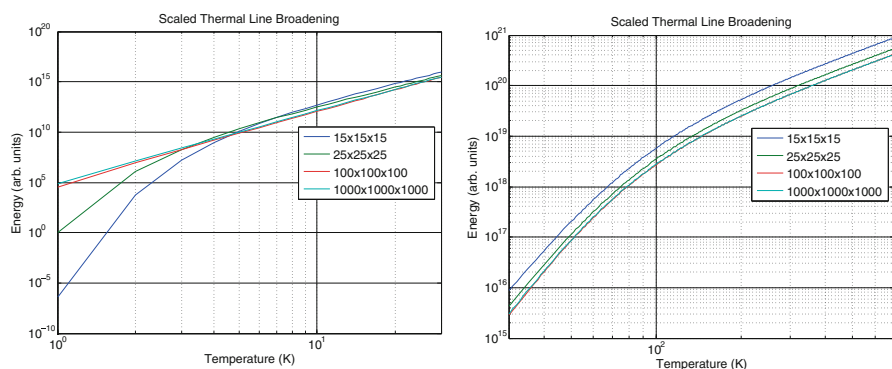
Fig. 4.7 Temperature dependence on the thermal broadening of a spectral line (given by the sum in Eq. (4.74)) for cubic nanoparticles ($15 \times 15 \times 15$-black, $25 \times 25 \times 25$-blue, $100 \times 100 \times 100$-red, $1000 \times 1000 \times 1000$-green) for temperatures ranges 1–30 K (*left*) and 30–700 K (*right*)
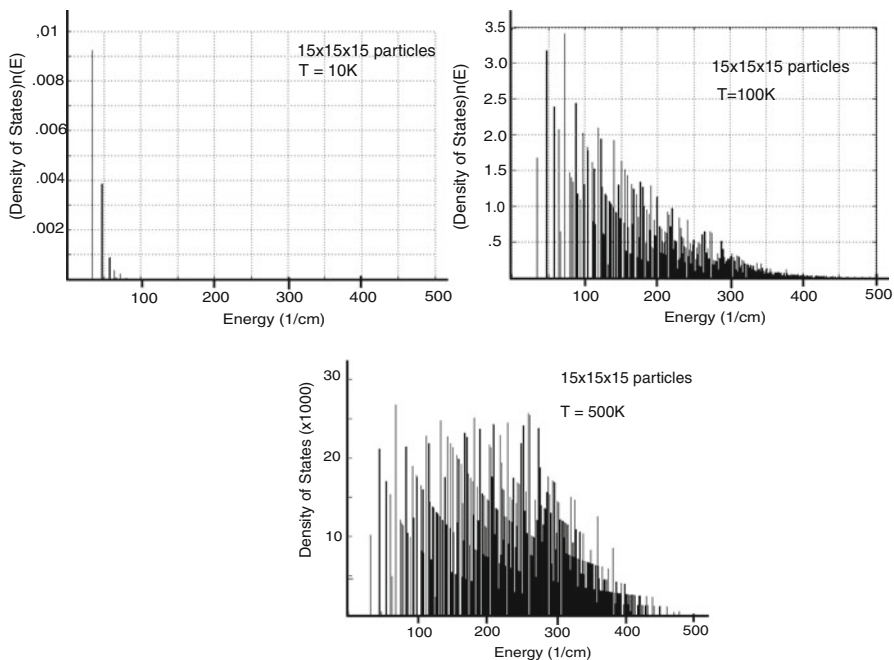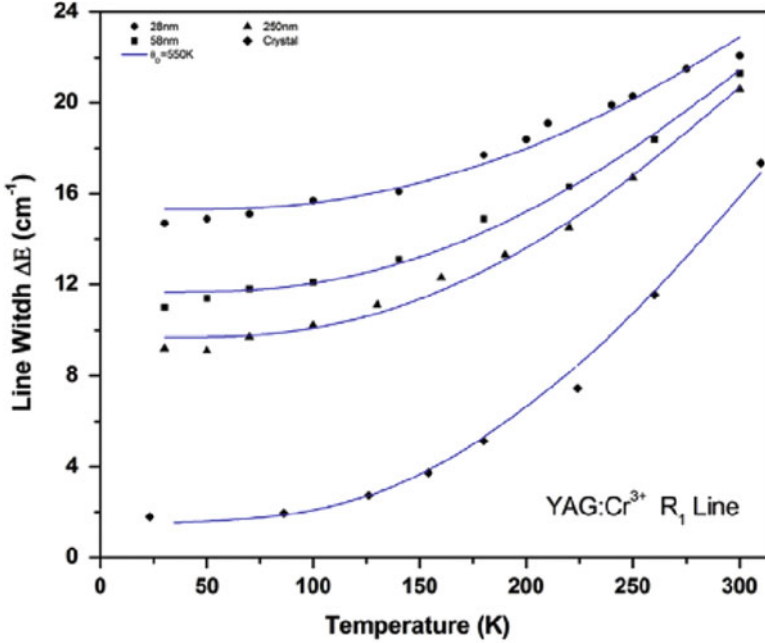
Fig. 4.8 Graphs showing the number of phonons as a function of phonon energy, i.e. $\varrho(\epsilon)n(\epsilon)$ *vs.* ϵ, for cubic nanoparticls $15 \times 15 \times 15$ atoms (size $\sim$3 nm) at T = 10, 100, and 500 K

The examples above show an unresolved conflict in the behavior of the electron-phonon coupling as the particle size changes. Whereas Meltzer et al. [21] suggest an increase in the coupling as the particle size decreases, the data from Erdem et al. [23] and Bilir et al. [24] suggest a decrease in the coupling as particle size decreases. And finally Suyver et al. [25] conclude that electron-phonon coupling is independent of particle size. These works indicate that a definitive answer as to how the electron-phonon coupling changes with particle size remains elusive.

4.9.2 Shifting of a Sharp Spectral Line in a Nanoparticle

The theoretical treatment of the thermal shift of the energy of the spectral line in a nanoparticle begins with Eq. (4.66) the shift due to a particular phonon mode, k.

$$\Delta\epsilon_{i,k} = \frac{\hbar}{Mv_s^2} \left[\left\langle \phi_i^0 \,\middle|\, V_2 \middle|\phi_i^0 \right\rangle + \sum_j \frac{\left|\left\langle \phi_i^0 \middle| V_1 \,\middle|\, \phi_j^0 \right\rangle\right|^2}{\epsilon_i - \epsilon_j} \right] \omega_k \left(2n_k + 1\right) \qquad (4.76)$$

Fig. 4.9 Linewidth vs. temperature of the R_1 line in nanopowders (●28 nm, ■58 nm, ▲250 nm), and in a single crystal (♦) of Cr-doped YAG. The solid lines are fits to Eq. (4.64) [23]

To find the total thermal shift of the particle, we neglect the contribution of spontaneous emission to (4.79) (i.e., $(2n_k + 1)$ becomes $(2n_k)$, and sum (4.79) over all phonon modes. Referring to (4.75) and (4.76), the total thermal shift can be written as:

$$\Delta\epsilon_i = \frac{2\hbar}{Mv_s^2}\left[\left\langle\phi_i^0\,\middle|\,V_2\middle|\phi_i^0\right\rangle + \sum_j \frac{\left|\left\langle\phi_i^0\middle|V_1\,\middle|\,\phi_j^0\right\rangle\right|^2}{\epsilon_i - \epsilon_j}\right]\sum_k g\left(\omega_k\right)\omega_k n_k \qquad (4.77)$$

The sum in (4.77) carries the temperature dependence of the thermal line shift. Figure 4.10 shows the fit the sum in Eq. (4.77) for cubic nanoparticles $(15 \times 15 \times 15,\ 25 \times 25 \times 25,\ 100 \times 100 \times 100,\ \text{and}\ 1000 \times 1000 \times 1000$ atoms) at temperatures between 1 K and 700 K. We see that, as with the line broadening, the main differences between the shift in large and small particles occurs at very low temperatures. At high temperatures, the thermal shift is nearly independent of particle size.

Erdem et al. studied the lineshift of the $^2E \rightarrow {}^4T_2$ emission line of Cr^{3+} in YAG in nanoparticles and in a bulk crystal [23]. The results showed that the thermal lineshift the lineshift decreases as the particle size decreases, which is consistent with Fig. 4.10. In that work, the lineshift was fit to Eq. (4.68) assuming a Debye
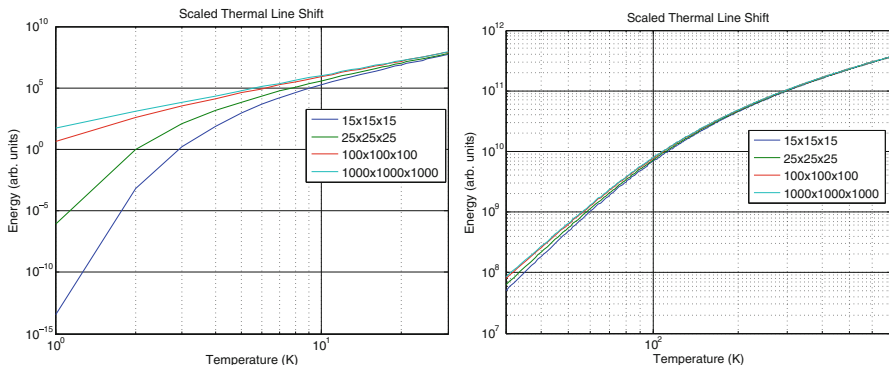
Fig. 4.10 Temperature dependence on the thermal shift of a spectral line (given by the sum in Eq. (4.78) for cubic nanoparticles ($15 \times 15 \times 15$-black, $25 \times 25 \times 25$-blue, $100 \times 100 \times 100$-red, $1000 \times 1000 \times 1000$-*green*) for temperatures ranges 1–30 K (*left*) and 30–700 K (*right*)

temperature of 550 K, and it was found that, as with the thermal line broadening data, the electron-phonon coupling parameter decreased with particle size. Given the lack of a theoretical explanation of the electron-phonon coupling decreasing with particle size, more work is required to say definitively why the shift is less in smaller particles.
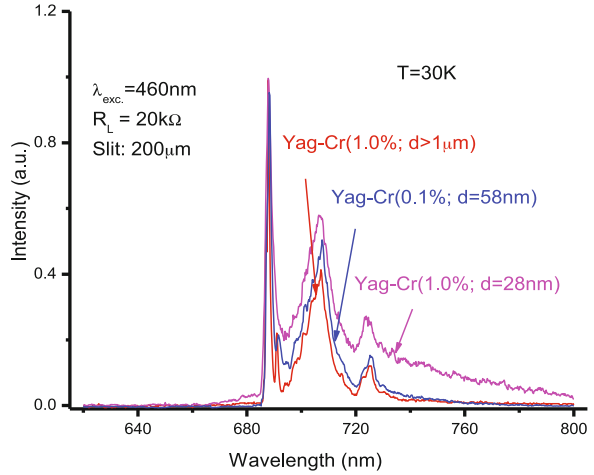
4.10 Vibronic Transitions

Following excitation, the decay of an isolated ion can occur via (4.1) emission of a photon, (4.2) emission of phonon(s), or (4.3) the emission of a photon concurrent with the absorption or emission of one or more phonons. This third process is referred to as a vibronic transition. In this section we discuss vibronic lines that appear as sidebands to a zero-phonon line in weakly-coupled systems [26–28].

### *4.10.1 Vibronic Sidebands of Sharp Lines: Theory*

In the limit of weak electron-phonon coupling, the narrow zero-phonon line is accompanied by sidebands, which result from the modulation of the zero-phonon transition by the vibrations of the solid. In Fig. 4.11, one immediately notices the rich structure contained in that sideband, structure that contains information of the phonon density of states. To explain such a structure, we must consider the interaction of the ion with the different phonon modes of the crystal.

The transition rate of a vibronic transition involving the emission of a photon and of a phonon in the *kth* mode is governed by terms having the following form:

Fig. 4.11 Emission spectra at 30K of Cr:YAG particles of 28 nm, 58 nm, and >1000 nm. Notice the broadening of the spectral lines and an enhanced background signal as the particle size decreases

Fig. 4.12 The vibronic emission process with states and transition operators labeled according to irreducible representations
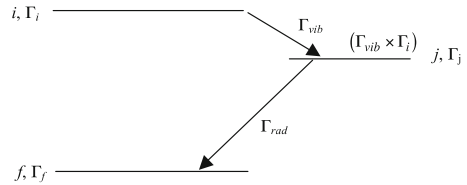
$$W_k \propto \left[\left| \langle \phi_f n_{k+1} | O_{ph} | \phi_j n_k \rangle \langle \phi_j n_k | O_{rad} | \phi_i n_k \rangle \right|^2 \right.$$

$$\left. + \left| \langle \phi_f n_{k+1} | O_{rad} | \phi_j n_k \rangle \langle \phi_j n_{k+1} | O_{ph} | \phi_i n_k \rangle \right|^2 \right] \tag{4.78}$$

where O_{rad} and O_{ph} in Eq. (4.78) represent the appropriate radiative and nonradiative operators and ϕ_i, ϕ_j, and ϕ_f are the wavefunctions of the initial, intermediate and final electronic states, respectively. The first term in Eq. (4.78) represents a process whereby a photon is created in the transition from the initial electronic state to an intermediate electronic state, and then a phonon is emitted in the transition to the final electronic state. The second term reverses the order of these transitions. Figure 4.12 shows a schematic drawing of a vibronic transition that represents by the second term in Eq. (4.78).

Each of the electronic wavefunctions and the operators have a certain symmetry, and using group theory one can associate them with certain irreducible representations. We make the following definitions.

Γ_i: the irreducible representation of the initial electronic state of the transition
Γ_f: the irreducible representation of the final electronic state of the transition
Γ_r: the irreducible representation of the radiative operator (We will assume that this is the electric dipole operator.)
Γ_v: the irreducible representation of the vibrational mode involved in the transition

Thus, for the vibronic transition shown in Fig. 4.12 to occur the direct product $\Gamma_i \times \Gamma_{vib} \times \Gamma_r$ must contain Γ_f:

$$\Gamma_f \in \Gamma_i \times \Gamma_v \times \Gamma_r \qquad (4.79)$$

We note that (82) is merely a selection rule, and can only be used to determine if a particular transition can occur; it cannot be used to determine the strength of a transition.

4.10.2   Vibronic Sidebands of Sharp Lines: The Case of Mgo:V^{2+}

Consider the case of a vibronic spectrum in emission at low temperature of MgO:V^{2+}, shown in Fig. 4.13 [28]. In MgO the V^{2+} ion sits in a site of octahedral symmetry, surrounded by six oxygen ions. Because the site has inversion symmetry, electric dipole transitions between two electronic states within the d^3 configuration are forbidden. As a result, the purely radiative transitions (accounting for the zero-phonon line) are driven by the magnetic dipole operator. Odd vibrations of the local complex destroy this inversion symmetry, so that the vibronic transitions involving such vibrations are electric dipole allowed.

We now examine the relationship between theses vibronic transitions in MgO:V^{2+} and the density of phonon states of the MgO lattice. First, we observe that the normal vibrational modes of the site symmetry of the octahedral group O_h are either purely even or purely odd. The representation of the final state (Γ_f) of the V^{2+} ion is known to be even. Since the electric dipole operator (Γ_{rad}) is odd, then a transition from the intermediate state via the electric dipole, according to Eq. (4.79), will be allowed only if the intermediate state is odd. The initial (excited) electronic state of V^{2+} is also even, so that only odd vibrations will be involved in the transition from Γ_i to Γ_j. Thus, Eq. (4.79) reduces to a statement of the parity selection rule.

It can be shown that of the phonons modes featured most prominently in the density of states of MgO, most of them can induce the octahedral complex to oscillate in one or more of its odd vibrational modes [29]. As a result, nearly all of the crystal phonon modes are able to participate in the vibronic transitions. The phonon spectrum of the MgO crystal (obtained by neutron scattering data [30]) is shown in Fig. 4.13a. The similarity of the shape of the low temperature vibronic sideband (Fig. 4.13b) to that of the phonon spectrum is striking, and suggests that the vibronic sideband can be closely related to the phonon spectrum of the lattice. That these two spectra show similarities and the fact that nearly all phonon modes of the MgO crystal can cause local vibrations to participate in the transition is not coincidental. However, proving that there is a one-to-one correspondence between the peaks (and valleys) of the two spectra is not trivial, since that would require

calculating the transition probabilities for each of the 3N-6 normal modes of the
crystal. Even if such a calculation could be done, it is no guarantee that such a
calculation would be able to reproduce the observed vibronic spectrum. Generally,
the shape of the vibronic spectrum will not exactly mimic that of the density of
phonon states. It is, however, a practical way of gaining insight into the phonon
density of states for some crystals.

In nanocrystals, where the confinement on the density of phonon states is most
severe, one would expect that changes to the density of states would be obvious in
the vibronic spectrum of the nanoparticle. In fact, such a result would represent the
most direct experimental evidence of the reduced density of states in nanoparticles.
Unfortunately, there is a significant amount of broadening of the zero-phonon line
in small nanocrystals, due to the fact that zero phonon lines from various sites
(due to the proximity of the surface) are shifted in energy with respect to one
another. The sum of the contributions from various sites overlaps with a large
portion of the phonon sidebands of the zero phonon line from the "normal" site.
An example of this is shown in the vibronic spectra of Cr-doped YAG nanoparticles
shown in Fig. 4.11. Perhaps due to the fact that this overlap is most prominent near

Fig. 4.13 (**a**) The density of states of MgO as determined from neutron scattering shown with (**b**) the vibronic sideband of MgO:V^{2+} [29]
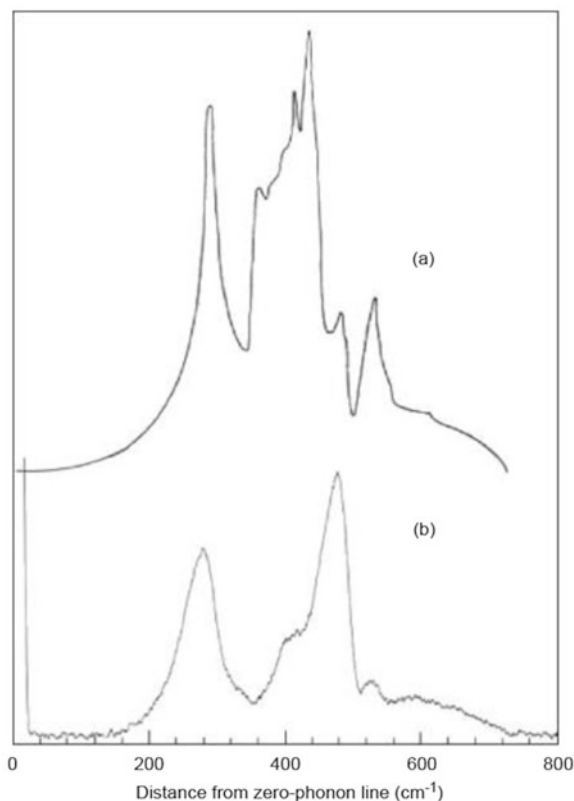
in the low energy range of the sidebands, where the most obvious changes (i.e., discreteness of the density of states and absence of the very low energy modes) to the density of states occur, there is no reported vibronic spectrum that clearly shows the vibronic spectrum changing with particle size. The difficulty in observing this is also complicated by the fact that the emission from nanoparticles is often very weak, probably because of the large number of surface states.

4.11   Conclusions

This paper first presented a detailed discussion of the Adiabatic Approximation(s), and the breakdown of that approximation, which allows for the existence of non-radiative processes. The electron-phonon coupling terms for the different adiabatic approximations were then discussed. This electron-phonon coupling was then used to determine the thermal broadening and shifting of sharp spectral lines of optically active ions in bulk solids. Integral to the broadening and shifting of spectral lines, and indeed to most non-radiative processes, is the phonon density of states in the system under investigation. Given that one goal of the paper was to examine how non-radiative processes depend on particle size, we then investigated how the phonon density of states depended on particle size. This investigation consisted of calculations of the phonon density of states for cubic nanoparticle, where it was found that for very small particles, the phonon density of states becomes very different than for bulk particles. The most obvious change in the phonon density of states between macro and nano systems occurs at the low energy end of the spectrum. After presenting this extensive background, the question of how non-radiative processes in doped insulators are altered as the size of the particles change from macroscopic to nano-sized was considered.

The fact that the electronic states of optically active ions in insulators are highly localized to the site of the ion, the general theory of non-radiative transitions is largely unaltered as the particle size changes. Using the calculated densities of states for cubic nanoparticles, we examined the thermal broadening and shifting of spectral lines for various particle sizes over a wide temperature range. Initial results hint that the effects of particle size on the broadening and shifting of lines are most likely to be observed only at low temperatures and in very small particles. Even in particles on the order of 50 nm, one is unlikely to be able to discern any contribution to these processes due to confinement effects of the phonon density of states. Also discussed were how the reduced phonon density of states inhibits the systems ability to reach thermal equilibrium and should changes in the vibronic sidebands in weakly-coupled systems.

References

1. Born, M., & Fock, V. (1928). *Zeitschrift für Physik, 51*, 165–180.
2. Born, M., & Oppenheimer, R. (1927). *Annals of Physics, 84*, 457.
3. Born, M., & Huang, K. (1956). *Dynamical theory of crystal lattices*. Oxford: Oxford University Press.
4. Henderson, B., & Imbusch, G. (2006). *Optical spectroscopy of inorganic solids*. Oxford: Oxford University Press.
5. Demtröder, W. (2005). *Molecular physics: Theoretical principles and experimental methods*. Weinheim: Wiley Press.
6. Azumi, T., & Matsuzaki, K. (1977). *Photochemistry and Photobiology, 25*, 315–326.
7. Ballhausen, C., & Hansen, A. (1972). *Annual Review of Physical Chemistry, 23*, 15.
8. Di Bartolo, B. (1976). Interaction of radiation with ions in solids. In B. Di Bartolo (Ed.), *Luminescence of inorganic solids*. New York: Plenum Press.
9. Herzberg, G. (1966). *Electronic spectra of polyatomic molecules*. Amsterdam: van Nostrand Press.
10. Wang, X., Dennis, W. M., & Yen, W. M. (1992). *Physical Review B, 46*(13), 8168–8172.
11. Tobert, W. M., Dennis, W. M., & Yen, W. M. (1990). *Physical Review Letters, 65*(5), 607–609.
12. Frenkel, J. (1931). *Physical Review, 37*, 17–44.
13. Struck, C. W., & Fonger, W. H. (1976). *Journal of Luminescence, 14*, 253–279.
14. Struck, C. W., & Fonger, W. H. (1975). *Journal of Luminescence, 10*, 1–30.
15. McCumber, D. E., & Sturge, M. D. (1963). *Journal of Applied Physics, 34*, 1682–1684.
16. Di Bartolo, B., & Peccei, R. (1965). *Physical Review, 137*(6A), 1770–1776.
17. Ellens, A., Andres, H., Meijerink, A., & Blasse, G. (1997). *Physical Review B, 55*(1), 173–179.
18. Ellens, A., Andres, H., Meijerink, A., & Blasse, G. (1997). *Physical Review B, 55*(1), 180–186.
19. Liu, G. K., Chen, X. Y., Zhuang, H. Z., Li, S., & Niedbala, R. S. (2003). *Journal of Solid State Chemistry, 171*, 123–132.
20. Liu, G. K., Zhuang, H. Z., & Chen, X. Y. (2002). *Nano Letters, 2*, 535.
21. Meltzer, R., & Hong, K. (2000). *Physical Review B, 61*(5), 3396–3403.
22. Takagahara, T. (1996). *Journal of Luminescence, 70*, 129–143.
23. Erdem, M., Ozen, G., Yahsi, U., & DiBartolo, B. (2015). *Journal of Luminescence, 158*, 464–468.
24. Bilir, G., Ozen, G., Collins, J., & Di Bartolo, B. (2014). *Applied Physics A, 115*(1), 263–273.
25. Suyver, J., Kelly, J., & Meijerink, A. (2003). *Journal of Luminescence, 104*, 187–196.
26. Miyakawa, T., & Dexter, D. L. (1970). *Physical Review B, 1*, 2961–2969.
27. Auzel, F. (1978). Multiphonon interaction of excited luminescent centers in the weak coupling limit: Non-radiative decay and multiphonon sidebands. In B. Di Bartolo (Ed.), *Luminescence of inorganic solids*. New York: Plenum Press.
28. Wall, W., Di Bartolo, B., Collins, J., & Orucu, H. (2009). *Journal of Luminescence, 129*(12), 1782–1785.
29. Wall, W. (1974). Ph.D. thesis, Boston College.
30. Sangster, M. J., Peckham, G., & Saunderson, D. H. (1970). *Journal of Physics C, 3*, 1026.